Solid State Communications 149 (2009) 2065–2069

Contents lists available at ScienceDirect

Solid State Communications

journal homepage: www.elsevier.com/locate/ssc

Interfacial layer in $La_{0.95}Tb_{0.05}MnO_3$/Nb-$SrTiO_3$ heterojunction

Y.T. Zhang [a,b], C.C. Wang [a,c,*], X.M. Feng [b], M. He [a], H.B. Lu [a]

[a] Institute of Physics & Center for Condensed Matter Physics, Chinese Academy of Sciences, Beijing 100190, China
[b] School of Material Science & Engineering, Shaanxi University of Technology, Hanzhong 723003, China
[c] Institute of Superconducting and Electronic Materials, Wollongong University, Wollongong, NSW 2519, Australia

ARTICLE INFO

Article history:
Received 24 April 2009
Received in revised form
11 August 2009
Accepted 13 August 2009 by J. Zhu
Available online 19 August 2009

PACS:
73.90.1f
77.55.1f
81.15.Hi

Keywords:
A. $La_{0.95}Tb_{0.05}MnO_3$/Nb-doped $SrTiO_3$ heterojunction
B. Laser molecular beam epitaxy
D. Interfacial layer
D. Dielectric properties

ABSTRACT

In this work, we report the electrical transport and dielectric properties of the $La_{0.95}Tb_{0.05}MnO_3$/Nb-doped $SrTiO_3$ heterojunction fabricated by laser molecular beam epitaxy. The sample shows a grain-boundary like current–voltage (I–V) behavior and linear C^{-2}–V (C is capacitance) behavior in both forward and backward biases. These results are interpreted in terms of an interfacial layer which absorbs electrons from the film and substrate forming back-to-back Schottky barriers. Charge carriers trapped by the interfacial layer are found to follow an electric-field activated law. This work demonstrates the presence of the interfacial layer and indicates that this layer can play an active role in determining the properties of the heterojunction.

© 2009 Elsevier Ltd. All rights reserved.

1. Intruduction

Manganite heterojunctions have attracted much attention due to their importance in both basic physics and potential applications. In this system, the interface between manganite film and substrate plays a decisive role in determining the physical properties and functionality of the junctions. A rich variety of exotic phenomena such as positive colossal magnetoresistance [1], resistive switching [2], low-frequency negative capacitance [3], etc. were reported to be associated with the interface. A Schottky barrier caused by an energy band bending due to the difference of Feimi level between the film and the substrate has been widely demonstrated as a key interfacial effect and thus most reports concentrate on the current rectifying behavior. Besides, an interfacial layer (IL) termed the "dead layer" due to its insulating behavior and depressed magnetization was occasionally reported to have a significant influence on the magneto-transport properties of the system [4]. Actually, in analogy to a grain boundary, an IL, as a transition layer from one material to another, contains a large number of localized defect states which serve as acceptors. Charge carriers trapped by these acceptors can hop between trap sites giving rise to thermal, magnetic, and electric field-dependent mobilities and thus the IL may be another key interfacial effect in understanding the properties of the junctions. For this reason, we would prefer to refer to the layer as an interfacial layer rather than a "dead layer" to emphasize its active role on magneto-transport properties. Properties related to this layer such as space charge limited current in some case may prevail over the property associated with the Schottky barrier [5]. However, the report of IL in manganite heterojunctions is very limited. This might be because the formation of the IL depends not only on lattice mismatch, but also on fabricating parameters and especially on oxygen pressure. On the other hand, the hopping motions of trapped charges in IL not only make a contribution to electric conductivity, but also give rise to a dipolar effect known as universal dielectric response [6], hence, the IL is difficult to fully characterize by the conventional magneto-transport measurements. It is, therefore, expected that the dielectric technique, especially the complex impedance method might be a powerful tool in the characterization of the IL. We herein reported the dielectric properties of $La_{0.95}Tb_{0.05}MnO_3$/Nb-doped $SrTiO_3$ (LTMO/SNTO) heterojunction. The Tb-doped $LaMnO_3$ was chosen because the dielectric properties of the doped $LaMnO_3$ are

* Corresponding author at: Institute of superconducting and electronic materials, Wollongong University, Wollongong, NSW 2519, Australia.
E-mail address: cwang@uow.edu.au (C.C. Wang).

0038-1098/$ – see front matter © 2009 Elsevier Ltd. All rights reserved.
doi:10.1016/j.ssc.2009.08.017

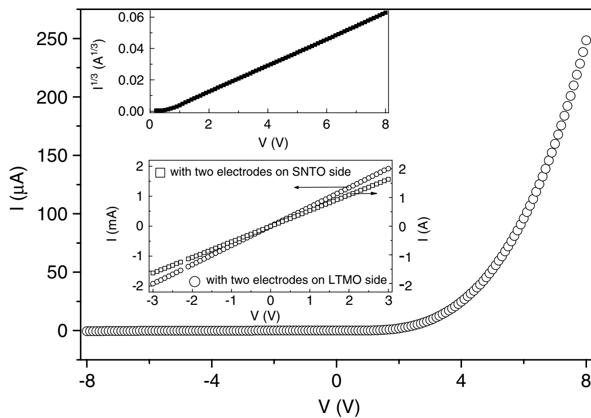

Fig. 1. I–V curve of the LTMO/SNTO heterojunction. Upper inset repolts the I–V curve for the forward bias with $I^{1/3}$ versus V. Lower inset presents the I–V curves measured with the two electrodes on the same side of the LTMO film and SNTO substrate.

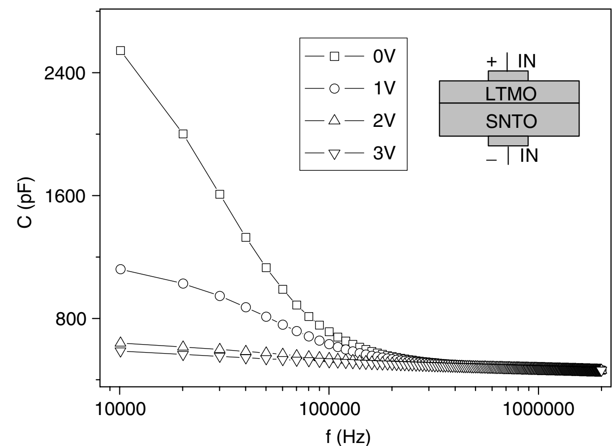

Fig. 2. The frequency dependence of the capacitance of the junction under various biases. The inset shows the layout for both electric and capacitance measurements.

characterized by the polaronic nature due to hopping charge carriers [7,8]. The mobile carriers are expected to be easily blocked at the interface between the film and substrate that allows for the formation of the IL. Our results convince the existence of this layer and indicate that both IL and Schottky effects are important factors in understanding the properties of the junction.

2. Experimental

Epitaxial LTMO thin films with a thickness of about 200 nm were deposited on (001) $SrNb_{1-x}Ti_xO_3$ substrate with the Nb doping level $x = 0.01$ by a computer-controlled laser molecular-beam epitaxy technique [9] using a XeCl laser ($\lambda = 308$ nm) with a pulse energy density of 2 J/cm^{-2} and a repetition rate of 2 Hz. At room temperature, the reflection peaks of bulk LTMO are consistent with a cubic perovskite with a pesudocubic lattice parameter of $a = 0.388$ nm [10], whereas the NSTO is cubic with the lattice parameter of 0.3905 nm. The in-plane lattice mismatch is −0.64%. To ensure the formation of IL, the oxygen partial pressure was kept at 2.3×10^{-1} Pa during the deposition and the substrate temperature kept at 630 °C. These parameters are much lower than those in the pulsed laser deposition process with frequently used values of several decades Pa and ∼800 °C, respectively. The former is expected to introduce oxygen vacancies into the film and the latter is expected to create defects in the film. Both are helpful for the formation of the IL. After the deposition, the samples were annealed *in situ* for 30 min under the deposition conditions and then cooled down to room temperature. The current–voltage (I–V) curve was measured by a Keithley 2400 source meter with a two point method. Dielectric properties were measured using an Agilent 4294 A precision impedance analyzer with indium slats (∼2 mm^2) well pressed on LTMO and SNTO as top and bottom electrodes, respectively. The voltage polarity was defined at the top electrode. The layout for both I–V and dielectric measurements was illustrated as the inset of Fig. 2. All measurements were carried out at room temperature.

3. Results and discussion

The I–V characteristic of the heterojunction displayed in Fig. 1 shows good rectifying behavior. It is well known that the rectifying behavior of a junction is due to the energy band bending that causes built-in fields as well as corresponding barriers at the interfaces. In our sample, three interfaces, In/LTMO, LTMO/SNTO, and SNTO/In may have contributions to the rectifying behavior. Ohmic contact of In/LTMO and NSTO/In was confirmed by the linear I–V behaviour measured with the two electrodes on LTMO and SNTO substrate (see the lower inset). Therefore the rectifying behavior can be identified as being related to the LTMO/SNTO heterojunction. Generally, such a nonlinear I–V behaviour is ascribed to the Schottky barrier formed in the SNTO side. The classic nonlinear conduction mechanisms for the Schottky barrier are the Schottky emission showing a linear relation of $\log I \propto V^{1/2}$, or its modified version [11] with a linear relation of $\log(I/V) \propto V^{1/2}$, and the Fowler–Nordheim tunneling [12] with $\log(I/V^2) \propto 1/V$. However, as seen from the upper inset of the figure, a perfect linear relationship between $I^{1/3}$ and V was obtained in a wide forward voltage range. This is a typical behavior of a varistor whose I–V relation is given by [13]

$$I \propto V^{\alpha} \quad (1)$$

where α is the non-linear coefficient ($\alpha = 2$ is known as space charge limited current). This fact clearly indicates that there exists a grain boundary-like IL. The I–V behavior of the junction is dominated by the IL instead of the Schottky effect.

Fig. 2 shows the frequency dependence of capacitance (C–f) of the junction under different forward biases. The low-frequency capacitance decreases rapidly with increasing frequencies indicating the interfacial polarization. Meanwhile, the low-frequency C–f curves can be greatly depressed by increasing biases. This fact further confirms the nature of interfacial polarization [14,15]. Based on the discussion of Fig. 1, the electrode contact effect can be neglected, the interfacial polarization, therefore, can be identified to be associated with the interface of the junction. On the other hand, the C–f curves become independent of both frequency and bias at frequencies higher than ∼500 kHz, indicating that the interfacial polarization has no evident contribution to the dielectric response above this frequency.

Fig. 3 presents the Nyquist plot, i.e., the imaginary part of the complex impedance $Z''(f)$ versus the real part $Z'(f)$, of the LTMO/NSTO junction under various biases (V). It can be clarified that each curve consists of two semicircular arcs. The low-frequency arc can be remarkably depressed by forward bias, convincing the nature of interfacial polarization [14]. At reversed biases, the impedance curves become almost bias-independent, and thus for the sake of clarity, the curves of $V = -2$ and -3 V are not shown in the figure. Generally, the low- and high-frequency arcs in the complex impedance plot represent the relaxations due to interfacial and bulk effects, respectively. We thus try to fit the data using an equivalent circuit as depicted by the lower inset in Fig. 3. The equivalent circuit consists of an uncompensated resistance (R_0) in series with two serially connected R-CPE units,

Table 1
Parameters obtained from the least-squares fittings for $R_i(V)$ based on Eq. (3).

Bias (V)	R_0 (Ω)	Bulk			Interface		
		R_b (Ω)	Q_b (Ω^{-1} m^{-2} S^{-n})	n_b	R_i (Ω)	Q_i (Ω^{-1} m^{-2} S^{-n})	n_i
3	7.12	1984.56	4.87×10^{-9}	0.96	63.32	3.81×10^{-7}	0.99
2	7.56	1540.09	5.24×10^{-9}	0.97	659.67	3.77×10^{-8}	0.95
1	8.34	1357.49	5.18×10^{-9}	0.97	2 337.14	2.69×10^{-8}	0.95
0	10.36	1389.46	4.92×10^{-9}	0.97	14 035.12	2.24×10^{-8}	0.98
−1	10.68	1391.81	4.90×10^{-9}	0.98	17 189.40	2.16×10^{-8}	0.98
−2	10.79	1384.31	4.87×10^{-9}	0.98	18 419.84	2.11×10^{-8}	0.98
−3	10.64	1382.84	4.86×10^{-9}	0.98	21 370.51	2.08×10^{-8}	0.98

Table 2
Fitting parameters of Fig. 4(a) based on Eqs. (3) and (4).

Frequency (Hz)	Backward bias						Forward bias					
	R_b (Ω)	R_{i0} (×10^{-11} Ω)	α (×10^{-2} C)	E_0 (eV)	C_b (nF)	C_i (nF)	R_b (Ω)	R_{i0} (×10^{-11} Ω)	α (×10^{-2} C)	E_0 (eV)	C_b (nF)	C_i (nF)
500	50.54	2.68	3.37	0.48	0.52	27.86	194.73	0.22	4.55	0.48	0.65	3.14
1 k	30.62	2.66	3.37	0.48	0.25	82.01	161.84	0.70	4.50	0.48	0.64	1.70
10 k	30.33	3.00	3.37	0.48	0.11	81.73	149.02	2.26	4.51	0.47	0.56	1.01
50 k	34.51	3.35	3.37	0.48	0.01	91.63	250.83	3.23	4.47	0.47	0.53	0.82
100 k	37.26	3.86	3.37	0.48	0.0028	106.29	292.02	3.49	3.63	0.48	0.51	0.33
500 k	40.07	4.43	3.37	0.48	0.0091	122.91	94.32	2.33	3.21	0.51	0.48	0.006

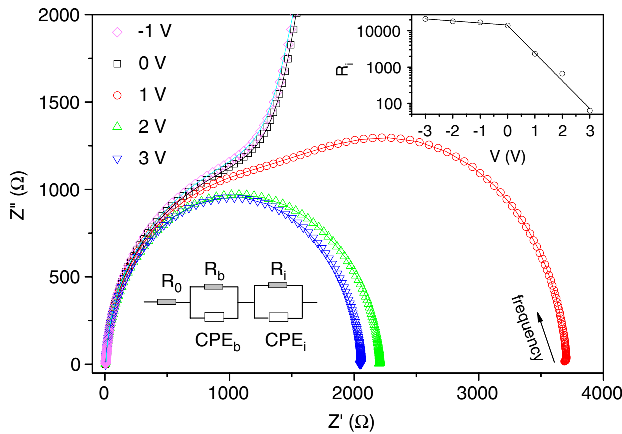

Fig. 3. Nyquist plot under different dc biases for the LTMO/SNTO heterojunction. The solid curves through data points are least-squares fittings based on the equivalent circuit displayed in the lower inset; the yielding resistance of the IL is shown in the upper inset therein, the straight line is the fitting result based on Eq. (3).

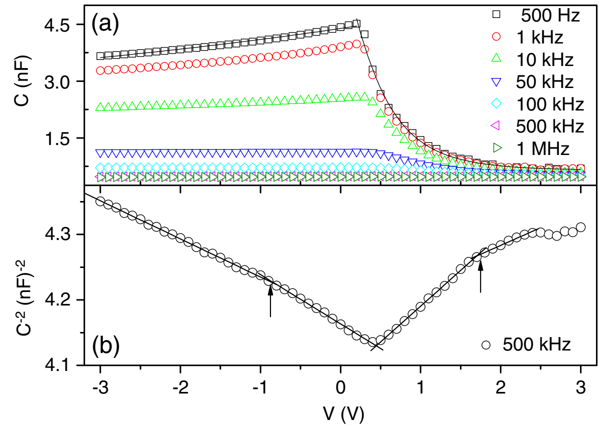

Fig. 4. (a) displays the C–V curves recorded at various frequencies for the LTMO/SNTO heterojunction. The solid curves are the least-squares fitting results to the data obtained at 500 Hz based on Eqs. (3) and (4). Fig. 4(b) replots the C–V curve of 500 kHz in Fig. 4(a) with the relation of C^{-2}–V. The straight lines are the results of linear fittings; the arrows indicate the crossover points of two segment lines.

one for the bulk and the other for interface, each containing a resistor (R) and a constant phase element (CPE) in parallel. The impedance of CPE is defined by [16]

$$1/Z_{\mathrm{CPE}} = Q(j\omega)^n \quad (2)$$

where ω $(= 2\pi f)$ is the angular frequency, j is the square root of -1, Q and n $(0 \le n \le 1)$ are adjustable parameters independent of the frequency. The fitted impedance curves shown as solid lines in Fig. 3 agree perfectly with the experimental data. The resultant parameters are listed in Table 1, from which we can see that the IL resistance, R_i, exhibits strong bias-dependence. As pointed out in Refs. [3,17], the bias dependence of $R_i(V)$ can be written as

$$R_i(V) = R_{i0}\exp[(E_0 - \alpha V)/k_B T] \quad (3)$$

where R_{i0} is a pre-exponential factor, E_0 is the activation energy at $V = 0$, and α is a constant. Fitting results based on Eq. (3) are shown as solid lines in the upper inset of Fig. 3. The fittings yield the parameters of $R_{i0} = 1.0 \times 10^{-4}$ Ω, $E_0 = 0.48$ eV, $\alpha = 1.5 \times 10^{-2}$ and 3.4×10^{-3} C in forward and backward regions, respectively. The efficacy of an applied bias is found to change the activation energy of the conductivity.

Fig. 4(a) displays the results of capacitance–bias (C–V) measurements of the junction. In the backward region, we note that the capacitance for all the measured frequencies increases slowly as the bias trends to zero, reflecting the fact that the impedance curve is almost independent of the bias in this region. While in the forward region, the C–V behavior depends strongly on the measuring frequency. In the frequency range $f \le 100$ kHz, the capacitance decreases drastically with the bias; whereas at frequencies higher than 100 kHz, the capacitance decreases slowly with the bias. This behavior is very similar to that of the $R_i(V)$ indicating that the C–V behavior is intimately linked with the interfacial polarization. We thus can quantitatively describe the C–V curve using the fitting equivalent circuit. In order to simplify the problem, only the two R-CPE units were considered and the CPEs were replaced by ideal capacitors [corresponding to $n = 1$ in Eq. (2)]. The capacitance of the system then can be written as [18]

$$C(V) = \frac{R_b^2 C_b + R_i^2 C_i + \omega^2 R_b^2 R_i^2 C_b C_i (C_b + C_i)}{(R_b + R_i)^2 + \omega_2 R_b R_i (C_b + C_i)}. \quad (4)$$

At fixed frequencies, the capacitances of the bulk (C_b) and IL (C_i) are constants. As seen in Table 1, $R_b(V)$ can be regarded as

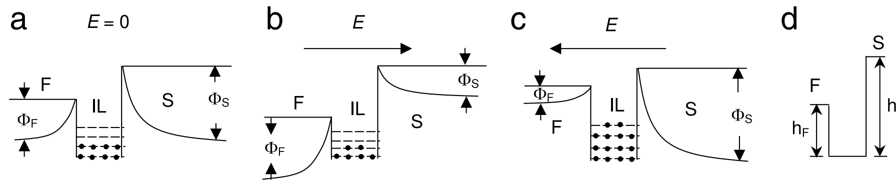

Fig. 5. Sketches of a grain-boundary like Schottky barrier under zero (a), forward (b), and backward (c) biases. Fig. 5(d) shows the schematic diagram of the asymmetric trap. (-•-: Trapped; —: Empty).

bias-independent when compared with $R_i(V)$. Taking Eqs. (3) and (4), the experimental data can be perfectly fitted as seen from the representative fitting curves at 500 Hz shown as solid lines in the figure. The resultant values of the fitting parameters are listed in Table 2. It is seen, however, that both resistances of the bulk and IL have a significant discrepancy from those deduced from the impedance analysis, which might be because the concentration of the space charge can be greatly tuned by scanning bias, whereas in the impedance measurements performed at a fixed bias, the concentration is almost invariable. This assumption is supported by the I–V hysteresis loop (not shown here), whose area can be regarded as a scale of the number of trapped carriers. It was found that the loop becomes smaller with faster voltage ramps. Nonetheless, several important aspects can be still extracted: (1) The values of E_0 and α agree very well with those deduced from the impedance analysis, indicating the field activated behavior is the same in both measuring modes. (2) The values of C_i in the backward region are much larger than those in forward region. This is because, as later discussed, the IL serves as a large capacitor in backward region. Meanwhile, a steep decrease in C_i at low frequencies is observed. This is because the stored carriers may transfer via tunneling, which leads to a notable decrease in C_i. Since tunneling is a slow charge transfer process, typically with the time constant of 10^{-3} s (the "waiting" time for the carriers before tunneling) which corresponds to a cutoff frequency of around 1 kHz [19,20]. Thus, when the testing a frequency lower than 1 kHz, a steep decrease in C_i can be seen. (3) In the forward region, C_b is almost frequency-independent, whereas C_i decreases notably with an increasing frequency. At a critical frequency of ~72 kHz, the bulk polarization takes over the interfacial polarization. At 500 kHz, C_i can be neglected when compared with C_b, reflecting the fact that interfacial polarization has no detectable contribution to the dielectric response above this frequency as indicated in Fig. 2.

Fig. 4(b) shows a typical C^{-2}–V curve obtained at 500 kHz, a frequency above which the interfacial polarization can be neglected. In both backward and forward regions, it is seen that the C^{-2}–V curve exhibits two linear lines with a demarking voltage around −0.8 and 1.7 V, respectively. Theoretically, the linear relationship between of C^{-2} and V is characteristic of the Schottky barrier in the reversed bias range [21]. The C^{-2}–V linear behavior found in both forward and backward biases implies that the Schottky effect alone is not sufficient to describe our results.

Considering the presence of the IL, we proposed a grain-boundary like Schottky barrier of the junction in Fig. 5. Since the film was grown in a very low oxygen pressure, a large amount of oxygen vacancies may be introduced into the film as confirmed by our previous results [22]. Hall measurements on another $La_{0.8}Tb_{0.2}MnO_3$ revealed a Hall coefficient of −7.671 cm^3/C, and a carrier density of 1.191×10^{18} cm^{-3}. These results also support our point. These vacancies act as donors and can release mobile electrons, while the heavily doped SNTO is usually considered as a degenerate n-type semiconductor. The IL possesses lots of localized defect states that attract electrons from both substrate (S) and film (F) forming a grain boundary-like barrier composed of two back-to-back Schottky barriers [23] with a barrier height of Φ_F and Φ_S in F and S, respectively [Fig. 5(a)]. The trapped charges in IL actually locate in an asymmetric potential with barrier heights of h_F and h_S near the F and S side, respectively [Fig. 5(d)]. Though the absolute value could not be defined, the quantitative evaluation $h_F < h_S$ can be obtained from the I–V behavior of Fig. 2. A positive bias lowers Φ_S while it enhances Φ_F [Fig. 5(b)]. In this case, the Schottky barrier in F is revise biased and hence shows C^{-2}–V linear behavior in the forward bias range. Meanwhile, h_F is also greatly depressed by the forward bias since the energy levels in the F side are greatly depressed by the bias, which leads to the exponential decrease in the number of the trapped carriers and in turn the great decrease in capacitance as seen in Fig. 4(a) and notable current in this bias range (Fig. 2). For higher forward biases, the ionization of the oxygen vacancies in F becomes evident, leading to a large leakage current and thus the C^{-2}–V curve deviates from the linear relation. In the reversed regime, Φ_S is enhanced while Φ_F is depressed. The linear behavior in C^{-2}–V curve in this regime is therefore related to the Schottky barrier of the substrate [Fig. 5(b)]. Because the resistance of SNTO substrate is many orders of magnitude lower than that of the film (see the lower inset of Fig. 1), the decrease in electric field takes place mainly within the film and IL. Therefore the barrier height h_S can be regarded as bias-independent, whereas h_F increases greatly with an increasing forward bias. In this case, Charge carries are trapped and stored at the IL and this layer actually serves as a large capacitor as already seen in Table 2. It is worth noting that the C^{-2}–V linear behavior in the backward bias range can be observed for all the testing frequencies from 500 Hz to 12 MHz. This is because the measured capacitance is the overall value of the capacitances of F, IL, and S collected in series, the large capacitance has less of a contribution to the total capacitance and hence has negligible influence on the C^{-2}–V behavior. While in the forward bias range, the C^{-2}–V linear behavior can only be observed at frequencies $f \geq 500$ kHz, confirming the fact that the space charge polarization can be neglected at this frequency. Finally it should be pointed out that the slope change of the C^{-2}–V curve causing two sectional linear behaviors might be related to the filling and emptying of deep traps. Details about this still await further investigation.

4. Conclusions

In conclusion, we demonstrate the existence of an interfacial layer in LTMO/NSTO heterojunction. This layer works like a grain-boundary, causing back-to-back Schottky barriers in LTMO film and NSTO substrate. Effects associated with the interfacial layer can be greatly tuned by an applied bias, which makes the properties of the junction bias sensitive. Our results indicate that both the interfacial layer and Schottky barrier play decisive roles on the properties of the junction, and the combination of the dielectric and electric techniques provides an effective way to characterize the interfacial properties of heterojunctions.

Acknowledgements

The authors acknowledge the financial support from the National Natural Science Foundation of China and the National Key Basic Research Programmer of China. This work was also supported by the China Postdoctoral Science Foundation.

References

[1] H.B. Lu, G.Z. Yang, Z.H. Chen, S.Y. Dai, Y.L. Zhou, K.J. Jin, B.L. Cheng, M. He, L.F. Liu, H.Z. Guo, Y.Y. Fei, W.F. Xiang, L. Yan, Appl. Phys. Lett. 84 (2004) 5007.
[2] S.Q. Liu, N.J. Wu, A. Ignatiev, Appl. Phys. Lett. 76 (2000) 2749.
[3] C.C. Wang, G.Z. Liu, M. He, H.B. Lu, Appl. Phys. Lett. 92 (2008) 052905.
[4] See, for example, J.Z. Sun, D.W. Abraham, R.A. Rao, C.B. Eom, Appl. Phys. Lett. 74 (1999) 3017;
M. Ziese, H.C. Semmelhack, K.H. Han, S.P. Sena, H.J. Blythe, J. Appl. Phys. 91 (2002) 9930;
R.P. Borges, W. Guichard, J.G. Lunney, J.M.D. Coey, F. Ott, J. Appl. Phys. 89 (2001) 3868.
[5] P.L. Lang, Y.G. Zhao, C.M. Xiong, P. Wang, J. Li, D.N. Zheng, J. Appl. Phys. 100 (2006) 053909.
[6] A.K. Jonscher, Dielectric Relaxation in Solids, Chelsea Dielectrics Press, London, 1983.
[7] A. Seeger, P. Lunkenhermer, J. Hemberger, A.A. Mukhin, V.Y. Ivanov, A.M. Balbashov, A. Loidl, J. Phys.: Condens. Matter. 11 (1999) 3273.
[8] C.C. Wang, L.W. Zhang, New J. Phys. 9 (2007) 210.
[9] G.Z. Yang, H.B. Lu, F. Chen, T. Zhao, Z.H. Chen, J. Cryst. Growth 227–228 (2001) 929.
[10] Y.T. Zhang, C.C. Wang, W.B. Liu, Z.H. Wang, H.B. Lu, Z.Y. Chen, Sci. China Ser. G: Phys. Mech. Astron. (in press).
[11] J.G. Simmons, Phys. Rev. Lett. 15 (1965) 967.
[12] M. Sze, Physics of Semiconductor Devices, 2nd ed., Wiley, New York, 1981.
[13] R. Bueno, J.A. Varela, E. Longo, J. Eur. Ceram. Soc. 28 (2008) 505.
[14] C.C. Wang, M. He, F. Yang, J. Wen, G.Z. Liu, H.B. Lu, Appl. Phys. Lett. 90 (2007) 192904;
G.Z. Liu, C. Wang, C.C. Wang, J. Qiu, M. He, J. Xing, K.J. Jin, H.B. Lu, G.Z. Yang, Appl. Phys. Lett. 92 (2008) 122903.
[15] M. Okutan, F. Azak, P. Sahin, M. Cavdarh, Z. Erdem, E. Senturk, Cryst. Res. Technol. 11 (2007) 1132.
[16] D. Morrison, D.J. Jung, J.F. Scott, J. Appl. Phys. 101 (2007) 094112.
[17] W. Li, R.W. Schwartz, J. Am. Ceram. Soc. 90 (2007) 3536.
[18] R. Stumpe, D. Wagner, D. Bauerle, Phys. Status Solidi (a) 75 (1983) 143.
[19] I. Lundström, C. Svensson, J. Appl. Phys. 43 (1972) 5045.
[20] A.B. Pakhomov, S.K. Wong, X. Yan, X.X. Zhang, Phys. Rev. B 58 (1998) R13375.
[21] H. Rhoderick, Metal-Semiconductor Contacts, Clarendon press, Oxford, 1980.
[22] S.H. Ouyang, C.C. Wang, G.Z. Liu, M. He, K.J. Jin, Z.M. Dang, H.B. Lu, Sci. China Ser. G: Phys. Mech. Astron. 51 (2008) 232.
[23] K. Eda, J. Appl. Phys. 49 (1978) 2964;
F. Greuter, G. Blatter, Semicond. Sci. Technol. 5 (1990) 111.